ChemComm

COMMUNICATION

Screening of the chemical reactivity of three different graphite sources using the formation of reductively alkylated graphene as a model reaction†

Kathrin C. Knirsch,[ab] Jan M. Englert,[ab] Christoph Dotzer,[ab] Frank Hauke[ab] and Andreas Hirsch*[ab]

Reductive alkylation of three graphite starting materials G(flake), G(powder), and G(spherical) reveals pronounced differences in the obtained covalently functionalized graphene with respect to the degree of functionalization, exfoliation efficiency and product homogeneity, as demonstrated by statistical Raman microscopy (SRM), TGA/MS, IR-spectroscopy and solubility behavior.

In 2004 graphene[1] joined the family of synthetic carbon allotropes as its youngest member.[2] This 2D form of carbon is currently at the forefront of nanoscience due to its outstanding and unprecedented materials properties.[3,4] A fundamental aim of carbon allotrope research is and has been the direct covalent functionalization[5–12] of the carbon framework. Generally, chemical functionalization can improve the solubility and processibility,[13] can modify the characteristic electronic and physical properties,[14,15] and allows for the combination of graphene properties with those of other compound classes.[16]

We have recently established a variety of covalent functionalization protocols[17–20] to access functionalized graphene in a top-down approach starting from graphite.[21] As there are many graphite sources available which can have quite different physical and morphological properties[22] we became interested in whether they also exhibit different behavior with respect to the chemical reactivity. Our survey is based on a basal plane alkylation[18] scenario employing the Na/K alloy as a reducing agent (Scheme 1).

Treatment of graphite with electropositive metals, such as potassium, is accompanied by reduction and yields the so-called graphite intercalation compounds (GICs).[23] Solvent driven exfoliation of the stacked crystals provides counter ion stabilized and reductively activated graphene sheets in solution. These graphenide[24] solutions can be subsequently trapped by electrophiles.
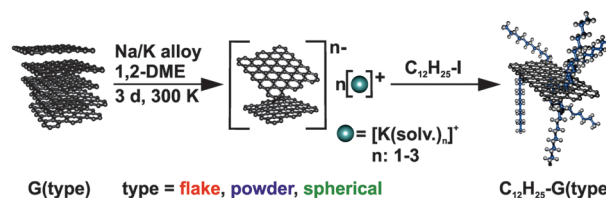
Scheme 1 Reductive exfoliation of graphite in 1,2-dimethoxyethane (DME) and subsequent addition of *n*-dodecyl iodide (prototype reaction) leading to alkylated graphene.

In the present study we focused on three different types of graphite (see Fig. 1 and Tables S1 and S2, ESI†): (a) G(flake) – a flake graphite with a particle size of 18 µm and a low intrinsic density of defects ($I_D/I_G \sim 0.2$), which is regularly stacked in contrast to powder graphite; (b) G(powder) – a powder graphite with a small particle size of 3–5 µm and some intrinsic disorder ($I_D/I_G \sim 0.3$) and (c) G(spherical) – a spherical, defect-rich graphite ($I_D/I_G \sim 0.4$), with a grain size of about 20 µm.

As a result of the morphological differences, the starting materials also vary in their bulk density (Fig. 1D). Specifically, G(powder) exhibits
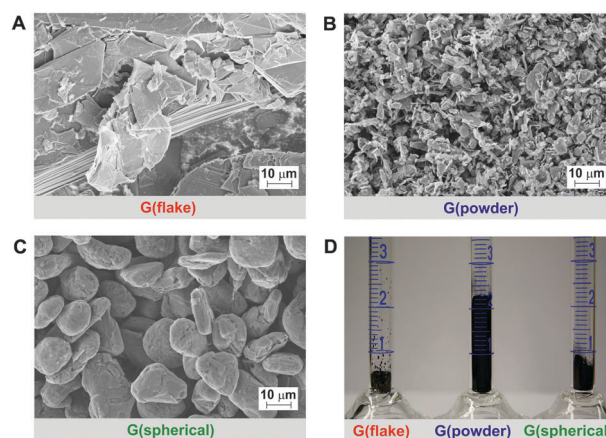
a Department of Chemistry and Pharmacy, University Erlangen-Nuremberg, Henkestrasse 42, D-91054 Erlangen, Germany. Fax: +49 9131 85 26864; Tel: +49 9131 85 22537

b Institute of Advanced Materials and Processes (ZMP), Dr-Mack-Strasse 81, D-90762 Fürth, Germany. E-mail: andreas.hirsch@fau.de; Fax: +49 911 6507865015; Tel: +49 911 6507865000

† Electronic supplementary information (ESI) available: Experimental procedures, additional Raman information, UV/vis details, IR-data, SEM-images, additional measurements and sample data. See DOI: 10.1039/c3cc46621c

Fig. 1 Starting graphite sources: SEM-images of (A) flake graphite, (B) powder graphite, (C) spherical graphite and illustration of (D) bulk density: G(flake) = 400 mg mL⁻¹, G(powder) = 90 mg mL⁻¹, and G(spherical) = 270 mg mL⁻¹.

the lowest bulk density in comparison to G(flake) and G(spherical).

The in-depth characterization of all materials has been carried out by statistical Raman microscopy (SRM)[20] and thermal gravimetric analysis. In general, in Raman spectroscopy the I_D/I_G-ratio can be taken as a measure for the amount of lattice anchor points introduced by the covalent functionalization sequence. The shape and the full width at half maximum (FWHM) of the characteristic 2D-band can be used to evaluate the graphene layers present. However, to ensure comparability of results, obtained from different samples, care has to be taken with respect to the statistical spread of the data. In particular, we found that bulk characterization of graphene is only reasonable by the application of a statistical analysis of the Raman data set.[20] For this approach at least 10 000 Raman spectra, obtained from a 10 000 μm^2 sized area of a graphenopaper – a free standing film generated by the filtration and drying of the functionalized material – have been recorded. This allows obtaining very representative information about the degree of functionalization (I_D/I_G-ratio), the homogeneity of the defect distribution and the exfoliation efficiency (FWHM$_{2D}$) of the different graphene layers. Based on the high reproducibility, valid conclusions on the bulk composition of the material can be deduced. In our case, we obtained consistent data from two individual alkylation sequences (see ESI,† Fig. S2). In Fig. 2, the SRM based histograms of C$_{12}$H$_{25}$-G(type) and of the respective starting materials (G(type)) are displayed together with the averaged spectra of the functionalized material (for further information, see Fig. S3, ESI†).

The histograms of the three graphites used as starting materials show a very similar I_D/I_G-ratio ($\sim$0.3) and a very narrow distribution. Compared to the starting materials, all functionalized samples exhibit a significant broadening of their I_D/I_G-ratio histograms. In the case of C$_{12}$H$_{25}$-G(powder) and C$_{12}$H$_{25}$-G(spherical), the Gaussian distribution of the obtained data follows the expected normal distribution function, while the I_D/I_G frequency distribution of C$_{12}$H$_{25}$-G(flake) covers the whole range from 0 to 4.5. This is indicative of the presence of a mixture of unfunctionalized graphite together with a broad distribution of covalently functionalized material with lower degrees of functionalization on average.
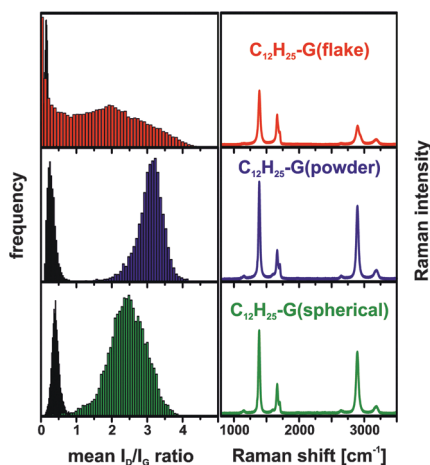
This analysis clearly shows that powder graphite represents a starting material which yields the highest degree of functionalization – $(I_D/I_G)_{average}$ = 3.1, corresponding to a mean inter-defect distance of approximately 5 nm.[20] This translates to about one addend per 850 framework C-atoms. The same analysis for the other two types of graphite together with the respective electrical characterization is given in the ESI,† Tables S3 and S4.

It should be emphasized that in the case of C$_{12}$H$_{25}$-G(powder) and C$_{12}$H$_{25}$-G(spherical) (Fig. S4, ESI†) a very sharp and symmetrical 2D-band with a mean FWHM of 35 cm^{-1} and 38 cm^{-1}, respectively, is observed (Fig. 4, right). These values are normally obtained for individualized monolayer graphene. In our case, the functionalized material was measured as a graphenopaper. In principle, during filtration of the functionalized graphene the respective individualized layers could re-aggregate. However, Raman spectra clearly show that exfoliated graphene layers are present, which is possible due to the addition of alkyl chains. The efficiency of the addend induced exfoliation depends on the number of C-atoms of the alkyl chain. In a series of n-(C$_n$H$_{2n+1}$)-G(powder) (n = 1–4, 6, 12, and 18) this trend becomes clearly evident (Fig. 3, also cf. ESI,† Fig. S5). In the case of n = 12 (dodecyl) and n = 18 (octadecyl) we observed the smallest FWHM of the 2D-band with 37 cm^{-1}.

In Fig. 4 (left) the distribution of the 2D-band widths is depicted as FWHM$_{2D}$ histograms. For C$_{12}$H$_{25}$-G(spherical), a slightly broader histogram can be determined, compared to the very narrow distribution of C$_{12}$H$_{25}$-G(powder). The very broad distribution in the case of the functionalized flake graphite (Fig. S6, ESI†) is indicative of a partial exfoliation of the starting material and did not permit a valid statistical analysis. This may be explained by the larger particle size of G(flake), which correlates with a higher intrinsic lattice energy, preventing an efficient exfoliation of the respective GIC.

For the determination of the nature of the covalently bonded addends mass spectrometric thermal gravimetric analysis (TGA/MS) was carried out (Fig. 5). Here, C$_{12}$H$_{25}$-G(powder) (blue trace) revealed the highest mass loss (-33.9%) in comparison to flake (-21.9%) and spherical graphite (-30.1%), respectively. Under the assumption that the total mass loss arises from the

Fig. 2 Left: Raman histograms (I_D/I_G-ratio) of the graphite starting materials (black) and reaction products (color coded). Right: averaged spectra (10 000 single point spectra) of dodecyl functionalized graphene, $\lambda_{exc.}$ = 532 nm.
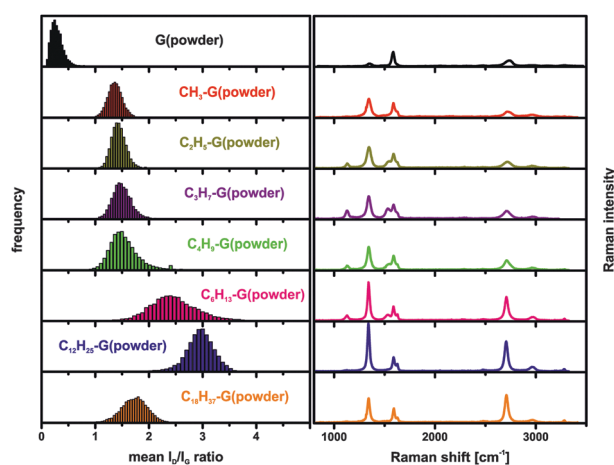

Fig. 3 Left: Raman histograms (I_D/I_G-ratio) of the starting material and the functionalized derivatives with n-alkyl chain length variation. Right: averaged Raman spectra, $\lambda_{exc.}$ = 532 nm.
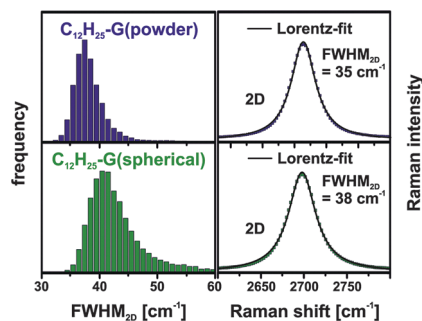
Fig. 4 Left: Raman histograms (FWHM$_{2D}$) of the functionalized materials (color coded). Right: averaged spectra (2D-band) of dodecyl functionalized graphene, $\lambda_{exc.}$ = 532 nm.

dodecyl addends, the degree of functionalization can be calculated to be 2.0% (C$_{12}$H$_{25}$-G(flake)), 3.6% (C$_{12}$H$_{25}$-G(powder)) and 3.1% (C$_{12}$H$_{25}$-G(spherical)), respectively. The amount of mass loss correlates with the Raman results. Thermal decomposition of the sample leads to the formation of volatile fragments, which are analyzed by mass spectrometry. Mainly, the detection of different alkyl-fragments, like the mass fragments m/z 85, 71, 57 and 43, is in line with a successful functionalization sequence.

For further characterization of the dodecyl functionalized material, infrared spectroscopy was also used. Convincing spectral information from the highly absorbing materials could only be obtained in transmission mode after dilution of the samples with potassium bromide from which pellets were produced for further analysis. Every functionalized sample clearly exhibits aliphatic C–H stretching vibrations, which is interpreted as indication of a successful alkylation (see Fig. S7, ESI†).

Also, the absorbance features of these carbon materials were analyzed by UV/vis spectroscopy. A suitable organic solvent providing high transmission into the UV range was found to be isopropanol, which in turn was used as a dispersing agent for the functionalized material (see Fig. S8, ESI†). The graphene samples were dispersed using an ultrasonication bath and left to sediment overnight to obtain clear solutions. All three types of graphite performed differently with respect to the level of absorbance (see Fig. S9, ESI†). The extinction coefficient of 24.6 mL mg^{-1} cm^{-1} at $\lambda = 660$ nm for dispersed graphene in solution determined by Hernandez et al.[25] was used to estimate the concentrations of the different samples, which vary from 3.00 µg mL^{-1} for C$_{12}$H$_{25}$-G(flake), 20.17 µg mL^{-1} for C$_{12}$H$_{25}$-G(powder) to 6.06 µg mL^{-1} for C$_{12}$H$_{25}$-G(spherical) (Fig. S9F and G, ESI†). Therefore, the functionalized powder graphite is, by far, more soluble than the functionalized flake and spherical graphite.
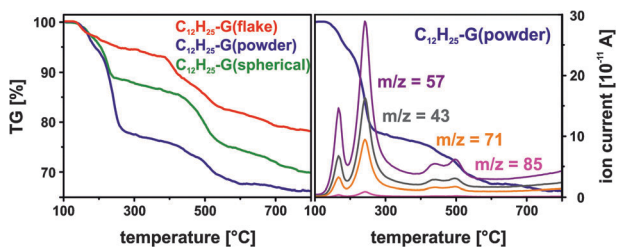

Fig. 5 TGA-mass loss of dodecyl functionalized graphene (mass loss of the starting material corrected).

To summarize, the chemical reactivity of graphite with respect to covalent functionalization strongly depends on the nature and in particular the morphology of the starting material. This was demonstrated by the generation of reductively alkylated graphene as a model reaction for the chemical functionalization of three different graphites. A detailed characterization of the reaction product in particular by statistical Raman microscopy (SRM) revealed significant differences with respect to the degree of functionalization, exfoliation efficiency and product homogeneity. Interestingly, the Raman spectra of dodecyl functionalized graphene samples, measured as a graphenopaper, clearly revealed a complete exfoliation and individualization of the graphene sheets and hence stabilization even in the solid state.

Notes and references

1 A. K. Geim and K. S. Novoselov, *Nat. Mater.*, 2007, **6**, 183–191.
2 A. Hirsch, *Nat. Mater.*, 2010, **9**, 868–871.
3 R. C. Haddon, *Acc. Chem. Res.*, 2013, **46**, 1–3.
4 K. F. Kelly and W. E. Billups, *Acc. Chem. Res.*, 2013, **46**, 4–13.
5 Z. Sun, D. K. James and J. M. Tour, *J. Phys. Chem. Lett.*, 2011, **2**, 2425–2432.
6 G. L. C. Paulus, Q. H. Wang and M. S. Strano, *Acc. Chem. Res.*, 2013, **46**, 160–170.
7 J. Park and M. Yan, *Acc. Chem. Res.*, 2013, **46**, 181–189.
8 A. Hirsch, J. M. Englert and F. Hauke, *Acc. Chem. Res.*, 2013, **46**, 87–96.
9 L. Rodriguez-Perez, M. a. A. Herranz and N. Martin, *Chem. Commun.*, 2013, **49**, 3721–3735.
10 V. Georgakilas, M. Otyepka, A. B. Bourlinos, V. Chandra, N. Kim, K. C. Kemp, P. Hobza, R. Zboril and K. S. Kim, *Chem. Rev.*, 2012, **112**, 6156–6214.
11 M. Quintana, E. Vazquez and M. Prato, *Acc. Chem. Res.*, 2013, **46**, 138–148.
12 J. Chattopadhyay, A. Mukherjee, S. Chakraborty, J. Kang, P. J. Loos, K. F. Kelly, H. K. Schmidt and W. E. Billups, *Carbon*, 2009, **47**, 2945–2949.
13 S. Eigler, M. Enzelberger-Heim, S. Grimm, P. Hofmann, W. Kroener, A. Geworski, C. Dotzer, M. Röckert, J. Xiao, C. Papp, O. Lytken, H.-P. Steinrück, P. Müller and A. Hirsch, *Adv. Mater.*, 2013, **25**, 3583–3587.
14 S. M. Kozlov, F. Viñes and A. Görling, *Adv. Mater.*, 2011, **23**, 2638–2643.
15 P. Huang, L. Jing, H. Zhu and X. Gao, *Acc. Chem. Res.*, 2013, **46**, 43–52.
16 H.-X. Wang, K.-G. Zhou, Y.-L. Xie, J. Zeng, N.-N. Chai, J. Li and H.-L. Zhang, *Chem. Commun.*, 2011, **47**, 5747–5749.
17 J. M. Englert, C. Dotzer, G. Yang, M. Schmid, C. Papp, J. M. Gottfried, H.-P. Steinrück, E. Spiecker, F. Hauke and A. Hirsch, *Nat. Chem.*, 2011, **3**, 279–286.
18 J. M. Englert, K. C. Knirsch, C. Dotzer, B. Butz, F. Hauke, E. Spiecker and A. Hirsch, *Chem. Commun.*, 2012, **48**, 5025–5027.
19 R. A. Schäfer, J. M. Englert, P. Wehrfritz, W. Bauer, F. Hauke, T. Seyller and A. Hirsch, *Angew. Chem., Int. Ed.*, 2013, **52**, 754–757.
20 J. M. Englert, P. Vecera, K. C. Knirsch, R. A. Schäfer, F. Hauke and A. Hirsch, *ACS Nano*, 2013, **7**, 5472–5482.
21 J. Malig, J. M. Englert, A. Hirsch and D. M. Guldi, *Electrochem. Soc. Interface*, 2011, **16**, 53–56.
22 N. V. Kozhemyakina, S. Eigler, R. E. Dinnebier, A. Inayat, W. Schwieger and A. Hirsch, *Fullerenes, Nanotubes, Carbon Nanostruct.*, 2013, **21**, 804–823.
23 A. Catheline, C. Valles, C. Drummond, L. Ortolani, V. Morandi, M. Marcaccio, M. Iurlo, F. Paolucci and A. Penicaud, *Chem. Commun.*, 2011, **47**, 5470–5472.
24 E. M. Milner, N. T. Skipper, C. a. Howard, M. S. P. Shaffer, D. J. Buckley, K. A. Rahnejat, P. L. Cullen, R. K. Heenan, P. Lindner and R. Schweins, *J. Am. Chem. Soc.*, 2012, **134**, 8302–8305.
25 Y. Hernandez, V. Nicolosi, M. Lotya, F. M. Blighe, Z. Sun, S. De, I. T. McGovern, B. Holland, M. Byrne, Y. K. Gun'Ko, J. J. Boland, P. Niraj, G. Duesberg, S. Krishnamurthy, R. Goodhue, J. Hutchison, V. Scardaci, A. C. Ferrari and J. N. Coleman, *Nat. Nanotechnol.*, 2008, **3**, 563–568.